



HAL
open science

Spin liquid state in a rare-earth hyperkagome lattice

J. Khatua, S. Bhattacharya, Q. Ding, S. Vrtnik, A. Strydom, N. Butch, H. Luetkens, Edwin Kermarrec, M. S. Ramachandra Rao, A. Zorko, et al.

► **To cite this version:**

J. Khatua, S. Bhattacharya, Q. Ding, S. Vrtnik, A. Strydom, et al.. Spin liquid state in a rare-earth hyperkagome lattice. *Physical Review B*, 2022, 106 (10), pp.104404. 10.1103/PhysRevB.106.104404 . hal-04311862

HAL Id: hal-04311862

<https://hal.science/hal-04311862>

Submitted on 28 Nov 2023

HAL is a multi-disciplinary open access archive for the deposit and dissemination of scientific research documents, whether they are published or not. The documents may come from teaching and research institutions in France or abroad, or from public or private research centers.

L'archive ouverte pluridisciplinaire **HAL**, est destinée au dépôt et à la diffusion de documents scientifiques de niveau recherche, publiés ou non, émanant des établissements d'enseignement et de recherche français ou étrangers, des laboratoires publics ou privés.

Spin liquid state in a rare-earth hyperkagome lattice

J. Khatua,¹ S. Bhattacharya,² Q. P. Ding,³ S. Vrtnik,⁴ A. M. Strydom,⁵ N. P. Butch,⁶ H. Luetkens,⁷
E. Kermarrec,² M. S. Ramachandra Rao,^{8,9} A. Zorko,^{4,10} Y. Furukawa,³ and P.Khuntia^{1,9,11,*}

¹*Department of Physics, Indian Institute of Technology Madras, Chennai 600036, India*

²*Université Paris-Saclay, CNRS, Laboratoire de Physique des Solides, 91405, Orsay, France*

³*Ames Laboratory, U.S. DOE, and Department of Physics and Astronomy, Iowa State University, Ames, Iowa 50011, USA*

⁴*Jožef Stefan Institute, Jamova c. 39, 1000 Ljubljana, Slovenia*

⁵*Highly Correlated Matter Research Group, Department of Physics, University of Johannesburg, PO Box 524, Auckland Park 2006, South Africa*

⁶*NIST Centre for Neutron Research, Gaithersburg, Maryland, USA*

⁷*Laboratory for Muon-Spin Spectroscopy, Paul Scherrer Institute, CH-5232 Villigen-PSI, Switzerland*

⁸*Department of Physics, Nano Functional Materials Technology Centre and Materials Science Research Centre, Indian Institute of Technology Madras, Chennai-600036, India*

⁹*Quantum Centre for Diamond and Emergent Materials, Indian Institute of Technology Madras, Chennai 600036, India.*

¹⁰*Faculty of Mathematics and Physics, University of Ljubljana, Jadranska u. 19, 1000 Ljubljana, Slovenia*

¹¹*Functional Oxide Research Group, Indian Institute of Technology Madras, Chennai 600036, India.*

(Dated: April 28, 2022)

Quantum fluctuations enhanced by frustration and subtle interplay between competing degrees of freedom offer an ideal ground to realize novel states with fractional quantum numbers in quantum materials that defy standard theoretical paradigms. Quantum spin liquid (QSL) is a highly entangled state wherein frustration induced strong quantum fluctuations preclude symmetry breaking phase transitions down to zero temperature without any order parameter. Experimental realizations of QSL in quantum materials with spin dimensionality greater than one is very rare. Here, we present our thermodynamic, nuclear magnetic resonance, muon spin relaxation and inelastic neutron scattering studies of a new rare-earth hyperkagome compound $\text{Li}_3\text{Yb}_3\text{Te}_2\text{O}_{12}$ in which Yb^{3+} ions constitute a three dimensional spin-lattice without any detectable disorder. Our comprehensive experiments evince neither signature of magnetic ordering nor spin freezing down to 38 mK that suggest the realization of dynamic liquid-like ground state in this antiferromagnet. The ground state of this material is interpreted by a low energy $J_{\text{eff}} = 1/2$ degrees of freedom with short range spin correlations. The present results demonstrate a viable basis to explore spin-orbit driven enigmatic correlated quantum states in a new class of rare-earth based three dimensional frustrated magnets that may open new avenues in theoretical and experimental search for spin liquids.

I. INTRODUCTION

Quantum materials wherein superposition and entanglement are at play may exhibit exotic physical phenomena, such as spin liquids with fractional quantum numbers coupled to emergent gauge field that offer a novel paradigm in advancing quantum science and technology [1–4]. The experimental realization of quantum spin liquid with exotic collective excitations in quantum materials set an outstanding track in modern condensed matter since the seminal proposal of P. W. Anderson in 1973 [5, 6]. Quantum spin liquids (QSLs) are characterized by absence of magnetic order down to $T = 0$, long-range entanglement, coherent fluctuation of spins and the preservation of local symmetries despite strong exchange interaction between spins [6–9]. Fractionalization of quantum numbers is a fingerprint of QSLs which are different from spin waves in conventional magnets. This is a well established scenario in one-dimensional (1D) magnets. It has been suggested that also 2D and 3D QSLs can host fractionalized deconfined quasiparticles such as spinons and

Majorana fermions the understanding of which is essential in advancing fundamental physics and is highly relevant for fault-tolerant quantum computing [6, 10–17]. However, the presence of perturbations, such as extra exchange couplings, unavoidable disorder, and defects in real materials put a strong constraint for the ideal realization of quantum spin liquids with $D \geq 2$ [18–20]. Moreover, 3D spin lattices that are composed of small triangular motifs in edge- or corner-sharing fashion, can host strong frustration similar to 2D spin lattices. Namely, quantum fluctuations in such 3D frustrated lattices with low value of spin could lead to unconventional ground states including spin liquids [11, 12]. This has motivated us to explore new quantum materials with rich potential to host such states with fractional quantum numbers [21–23]. The intertwining of spin-orbit coupling, anisotropy, spin correlations and frustration in rare-earth magnets offer another route to realize novel quantum states [4, 7, 24–26]. In recent years, spin-orbit driven frustrated magnets have provided a new light to realize novel quantum phenomena ranging from spin ice state [7, 27] to spin liquid [15, 24, 28] and anomalous and spontaneous Hall effect [29, 30] to Bose-Einstein condensate phase [25, 31]. In lanthanide magnetic materi-

* pkhuntia@iitm.ac.in

als, the interplay between spin-orbit coupling and low-symmetry crystal electric field leads to Kramers doublets where effective $J_{\text{eff}} = 1/2$ moments of rare-earth ions appear, contrary to pure $S = 1/2$ moments in transition metal ions. The 3D spin lattice based quantum magnets host a plethora of unconventional properties of 3D magnets including non-trivial short-range spin correlation [32], unconventional spin glass [33], and magnetic Coulomb phase [34, 35]. For example, the lanthanide family $A_2B_2O_7$ where rare-earth ions form a pyrochlore lattice is a rich reservoir that hosts a wide range of quantum phenomena owing to complex interplay between competing degrees of freedom [7, 36]. Quite recently, $Ce_2Zr_2O_7$ was proposed to be a 3D QSL candidate, where Ce^{3+} ions with $J_{\text{eff}} = 1/2$ moments decorate a network of corner-sharing tetrahedra [37]. The observation of $U(1)$ QSL and emergent phases driven by multipolar interactions in its analogue $Ce_2Sn_2O_7$ also set a unique example of a 3D spin-lattice for exploring quantum many-body phenomena [38]. Furthermore, the garnet series $R_3B_5O_{12}$ (R = rare-earth ions and B = Ga and Al) where the rare-earth ions decorate two interpenetrating hyperkagome lattices are known to harbor myriads of interesting quantum phenomena such as long-range multipolar state [39, 40] and Ising antiferromagnets [41, 42]. However, most of the garnets undergo a magnetic phase transition at lower temperature [43–49]. Therefore, the search for an ideal 3D spin lattice to realize a QSL state poses a particularly challenging problem. For example no report has been published so-far on a structurally perfect $4f$ -based hyperkagome lattice in which high degree of spin frustration and anisotropic interactions mediated by spin-orbit coupling could stabilize an enigmatic 3D spin liquid.

Here, we report a new rare-earth based quantum magnet $Li_3Yb_3Te_2O_{12}$ and investigate its inherent physics of 3D frustrated spin-lattice with $J_{\text{eff}} = 1/2$ moments of Yb^{3+} ions. $Li_3Yb_3Te_2O_{12}$ crystallizes in the cubic space group $Ia\bar{3}d$ where Yb^{3+} ions form an interpenetrating hyperkagome spin-lattice. Our thermodynamic results suggests the presence of a Kramers doublet state and antiferromagnetic interaction between $J_{\text{eff}} = 1/2$ spins at low temperature. The absence of long-range magnetic ordering and spin freezing down to at least 38 mK in our ac susceptibility, specific heat and NMR experiments is the first fingerprint of a spin liquid state in this frustrated quantum material. Furthermore, specific heat measurements show the presence of short-range spin correlations in this antiferromagnet. Our complementary experimental probes thus demonstrate a dynamic ground state and a field-induced gapped behavior in the spin excitation spectrum in this spin-orbit driven frustrated hyperkagome quantum material.

II. METHODS

Sample synthesis: Polycrystalline samples of $Li_3Yb_3Te_2O_{12}$ (henceforth LYTO) were synthesized by a standard solid-state reaction of Li_2CO_3 (99.0 %, Alfa Aesar), Yb_2O_3 (99.998 %, Alfa Aesar), and TeO_2 (99.9995 %, Alfa Aesar) [50]. Since the lanthanide-oxide and Li_2CO_3 are generally hygroscopic, before being weighed, Yb_2O_3 and Li_2CO_3 were preheated at 900°C and 100°C, respectively. The stoichiometric mixtures of starting materials were pelletised and heated at 800°C for 30 hours in air with several intermittent grindings. We also used Y_2O_3 (99.999 %, Alfa Aesar) and followed the same procedure to prepare the isostructural non-magnetic analogue $Li_3Y_3Te_2O_{12}$. The phase purity was checked by room temperature powder X-ray diffraction (XRD) using smartLAB Rigaku X-ray diffractometer with Cu $K\alpha$ radiation ($\lambda = 1.54 \text{ \AA}$). The crystal structure of LYTO was confirmed by the Rietveld refinement of X-ray diffraction data using GSAS software [51]. All the XRD peaks could be indexed with the cubic space group $Ia\bar{3}d$ and lattice parameter $a = 12.173 \text{ \AA}$ [50]. No secondary phase is detected in XRD and the Rietveld refinement of XRD data rules out the presence of any inter-site disorder between the constituent atoms. The observed sharp XRD peaks indicate high quality polycrystalline samples investigated in this work.

Magnetization measurements: Magnetization data were acquired using a Quantum Design, SQUID magnetometer in the temperature range $2 \text{ K} \leq T \leq 350 \text{ K}$. Magnetic susceptibility ($\chi(T)$) data were recorded in magnetic fields 0.1 and 1 T and the zero-field cooled (ZFC) and field cooled (FC) data were collected in a magnetic field of 0.01 T. In order to determine the effective magnetic moment (μ_{eff}) and Curie-Weiss temperature (θ_{CW}), the high-temperature ($>160 \text{ K}$) inverse susceptibility ($1/\chi(T)$) data were fitted with Curie-Weiss (CW) law $\chi = \chi_0 + C/(T - \theta_{\text{CW}})$. Here C is the Curie constant which is used to calculate $\mu_{\text{eff}} = \sqrt{8C} \mu_B$, χ_0 is the temperature independent paramagnetic susceptibility, and θ_{CW} provides an estimate of magnetic exchange interactions. The isotherm magnetization data are reproduced well (see SI Fig. 3) by a function of the form $M/M_s = B_{1/2}(y)$, where $B_J(y) = [\frac{2J+1}{2J} \coth[\frac{y(2J+1)}{2J}] - \frac{1}{2J} \coth \frac{y}{2J}]$ is the Brillouin function, $M_s (= gJ\mu_B)$ is the saturation magnetization and the parameter $y = g\mu_B J\mu_0 H/k_B T$, where μ_B is the Bohr magneton, g is the Landé g-factor. The Brillouin function fit with fixed $J = 1/2$ to magnetization data yields Landé g factor, $g = 3.54 \pm 0.02$.

Specific heat measurements: Specific heat measurements were performed in the temperature range $0.35 \text{ K} \leq T \leq 270 \text{ K}$ under magnetic fields $0 \text{ T} \leq \mu_0 H \leq 7 \text{ T}$, using thermal-relaxation technique provided by Quantum Design, PPMS. Furthermore, specific heat measurements were carried out separately in the temperature range $0.054 \text{ K} \leq T \leq 4 \text{ K}$ in zero-field using a dilution refrigerator which was also used to measure ac

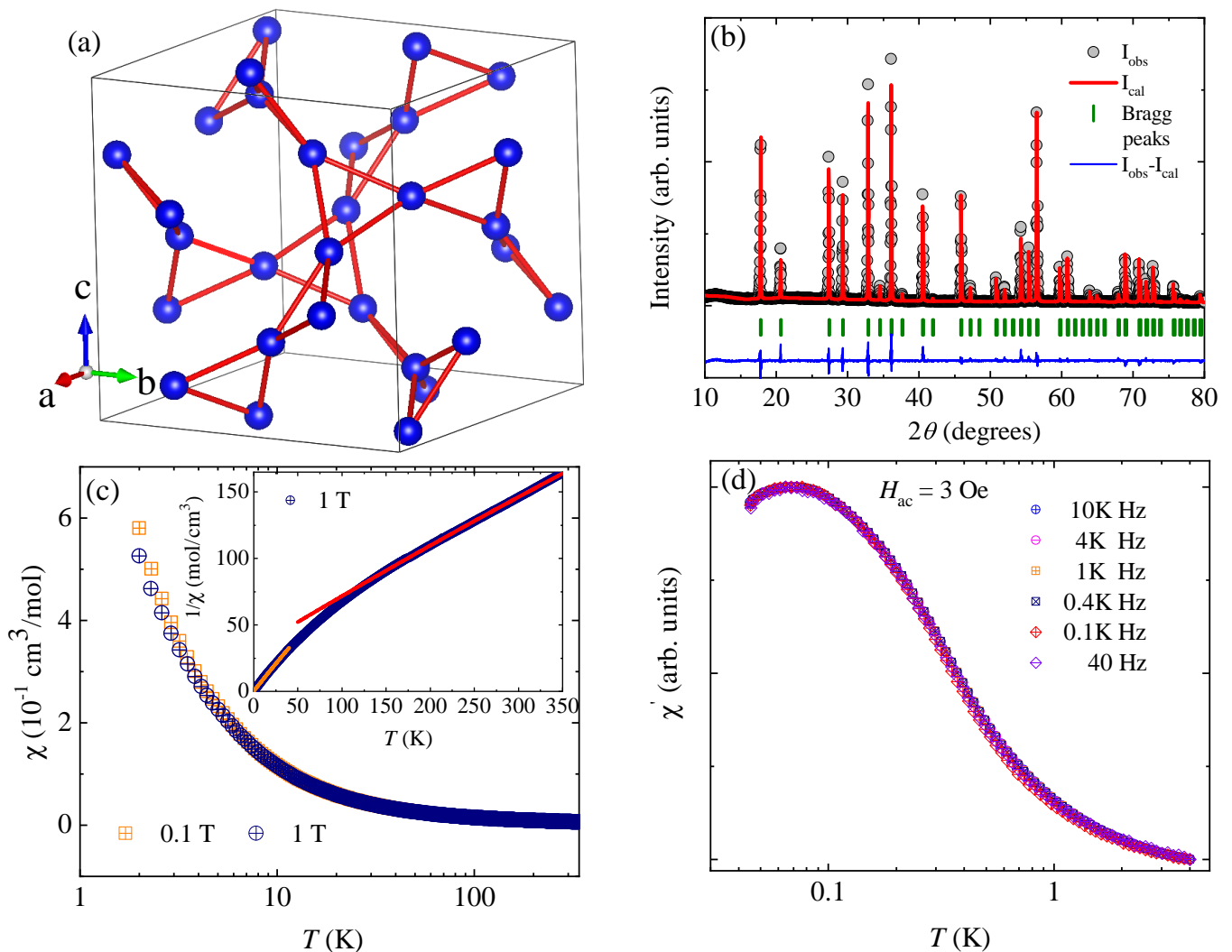


FIG. 1. Crystal structure and bulk magnetic properties of LYTO. (a) The position of the Yb^{3+} magnetic ions within the unit cell. These Yb^{3+} ions decorate two interpenetrating chains of 3D corner-shared triangles known as the hyperkagome lattice. (b) Rietveld refinement of powder X-ray diffraction data recorded at room temperature. The experimentally observed points (circles), the calculated Rietveld refinement profile (solid line), the Bragg reflection positions (olive vertical bars) and the difference between the observed and calculated intensity (blue line) are shown. (c) The temperature dependence of magnetic susceptibility in two magnetic fields. The inset shows the temperature dependent inverse magnetic susceptibility data with the orange and red lines showing the Curie-Weiss fits for the low- and high-temperature data, respectively. (d) The temperature dependence of the real part of ac susceptibility at different frequencies down to 45 mK.

susceptibility in the temperature range $0.045 \text{ K} \leq T \leq 4 \text{ K}$ at six different frequencies using a Dynacool PPMS instrument from Quantum Design. The total specific heat of LYTO can be expressed as a sum of contributions from the electronic spins in the ground state Kramers doublet (C_{mag}), lattice contribution (C_{lat}) and nuclear contribution (C_n) i.e., $C_{\text{tot}}(T) = C_{\text{mag}}(T) + C_{\text{lat}}(T) + C_n$. We also measured specific heat of the $\text{Li}_3\text{Y}_3\text{Te}_2\text{O}_{12}$ which we used as a non-magnetic analogue to subtract the lattice contribution. After subtraction lattice contribution, we subtracted nuclear Schottky contribution $C_n \propto T^{-2}$ to obtain magnetic specific heat.

NMR measurements: Field-swept ${}^7\text{Li}$ ($I = 3/2$, and

gyromagnetic ratio 16.54 MHz/T) NMR measurements down to 38 mK at several frequencies were carried out on a homemade phase-coherent spin-echo pulse spectrometer equipped with a 9 T Oxford magnet. The low temperature NMR measurements were performed with a Oxford Kelvinox dilution refrigerator. NMR spectra measurements were carried out using a standard Han-echo sequence while the spin lattice relaxation time measurements were performed following saturation-recovery method. In LYTO, ${}^7\text{Li}$ is an NMR active nucleus which couples with Yb^{3+} ions via hyperfine interactions. Therefore, ${}^7\text{Li}$ NMR can probe the intrinsic magnetic susceptibility as well as low-energy spin excita-

tions via spectrum position, and spin-lattice relaxation, respectively. The temperature dependence of the NMR shift (K) at different frequencies was extracted from the fit of field-swept NMR spectra. For an anisotropic magnetic material three different components of NMR shift $K(T)$ such as K_{iso} (isotropic shift), K_{ax} (axial shift) and K_{aniso} (anisotropic shift), arising from a general hyperfine coupling tensor, can be determined from the observed experimental line shape. In this respect, the principal components K_X , K_Y and K_Z of tensor $K(T)$ can be used to define $K_{\text{iso}} = 1/3(K_X + K_Y + K_Z)$, $K_{\text{aniso}} = 1/2(K_Y - K_X)$ and $K_{ax} = 1/6(2K_Z - K_X - K_Y)$ [52, 53]. The temperature dependence of the NMR shift scales with the magnetic susceptibility as $K_{\text{ax/iso}}(T) = K_0 + (A_{\text{hf}}^{\text{ax/iso}}/N_A\mu_B)\chi_{\text{spin}}(T)$, where K_0 is the temperature independent chemical and orbital shift, A_{hf} is the hyperfine coupling constant between ${}^7\text{Li}$ nucleus and Yb^{3+} spins, μ_B is the Bohr magneton and N_A is the Avogadro number, respectively. To extract the hyperfine couplings, the standard Clogston-Jaccarino plot (see SI Fig. 7) was used to fit in two temperature regimes and the obtained fitting parameters are given in SI note 5. The fit of NMR spectra below 1 K is not very good (see SI Fig. 6) which could be due to an additional spectral weight in the low-field side at low temperature, however, the origin is not clear at this moment. To uncover the dynamics of Yb^{3+} spins in LYTO at very low-energy, we conducted spin-lattice relaxation time measurement. In order to estimate T_1^{-1} , the recovery of longitudinal nuclear magnetization data were fitted by the single exponential function $M_z(t) = (M_0 - M(t))/M_0 = A \exp(-t/T_1)$ in the entire temperature range of the investigation, where M_0 is the equilibrium magnetization, $M_z(t)$ is the magnetization at time t after the saturation pulse and A is a constant. The validity of a single exponential function in a wide temperature range suggests that the electronic moments are uniformly distributed in the host lattice without disorder. The fits of the recovery curves with a formula for $I = 3/2$ nuclei were not as good as the single exponential function.

μSR : Muon spin relaxation measurements were performed at the Paul Scherrer Institute, on the GPS instrument. A weak transverse field of 50 Oe was applied to determine the initial asymmetry parameter. Zero-field (ZF) and longitudinal applied fields (LF) datasets were obtained using VETO mode resulting in minimal background signal (< 0.02).

Inelastic neutron scattering: Time-of-flight inelastic neutron scattering measurements were carried out at the NIST Center for Neutron Research (NCNR, Gaithersburg, MD) on the DCS spectrometer. In order to isolate the field evolution of the inelastic spectrum, a field-independent background, made of the average of the 0 and 2T datasets for $E > 0.85$ meV and of the average of the 7, 8, 9 and 10 T datasets for $E < 0.85$ meV, was subtracted from the Q -integrated energy cuts. Simulations of powder-averaged dynamical

structure factor for inelastic neutron scattering were done with the SpinW software [54].

III. RESULTS

A. Magnetization

The magnetic susceptibility $\chi(T)$ data do not exhibit any signs of a magnetic phase transition down to 2 K (Fig. 1 (c)). The Curie-Weiss (CW) fit to the high-temperature (>160 K) $\chi(T)$ data yields $\theta_{\text{CW}} \approx -78$ (1) K, $\mu_{\text{eff}} = 4.4 \mu_B$, which is close to $\mu_{\text{eff}} = 4.54 \mu_B$ of a free Yb^{3+} ($J = 7/2$) spin and $\chi_0 = 4.97 \times 10^{-4} \text{ cm}^3/\text{mol}$. The estimated large negative θ_{CW} is ascribed to the energy scale of excited crystal electric field levels [24]. The interaction energy scale of $4f$ systems is much lower and is in our case revealed at low-temperature where the CW fit of $1/\chi(T)$ data in the temperature range $2 \text{ K} \leq T \leq 10 \text{ K}$ yields $\mu_{\text{eff}} = 3.0 \mu_B$ and $\theta_{\text{CW}} \approx -0.3 \text{ K} \pm 0.03 \text{ K}$. The obtained effective moment is smaller than the Yb^{3+} free-ion value, which suggests a Kramers doublet state at low temperature, as also confirmed by specific heat measurements (see below). The negative CW temperature indicates antiferromagnetic interactions between the pseudo $1/2$ moment of Yb^{3+} ions with approximate interaction energy of the order of θ_{CW} . The Curie-Weiss temperature of most $4f$ systems is typically small and thus the onset of spin correlation develops at very low temperature in these quantum materials [37, 38, 42, 55, 56]. Furthermore, the absence of any bifurcation in zero-field cooled (ZFC) and field cooled (FC) susceptibility data (see SI Fig. 2) in the field of 100 Oe suggests that Yb^{3+} spins are not frozen down to 2 K. In order to confirm the absence of spin freezing, we performed ac susceptibility measurement down to millikelvin temperatures at different frequencies. Fig. 1 (d) depicts the real part of ac susceptibility as a function of temperature down to 45 mK and it exhibits a broad maximum around 80 mK which suggests the short range interaction between Yb^{3+} moments in LYTO [57–59]. Importantly, the absence of any frequency dependency of ac susceptibility strongly rules out glassy behavior of Yb^{3+} spins in LYTO. The magnetization isotherms at a few selected temperatures are shown in SI Fig. 3 and the absence of any visible hysteresis rules out the presence of any ferromagnetic signal. The calculated Landé g factor, $g = 3.46 \pm 0.02$, from the low-temperature Curie-Weiss fit of magnetic susceptibility, is close to that obtained Landé g factor from Brillouin function fit of the magnetization isotherm. A similar value of powder average of Landé g factor is also observed in Yb based 3D pyrochlore system suggesting the single-ion properties of LYTO are expected to be similar to the pyrochlore system [58].

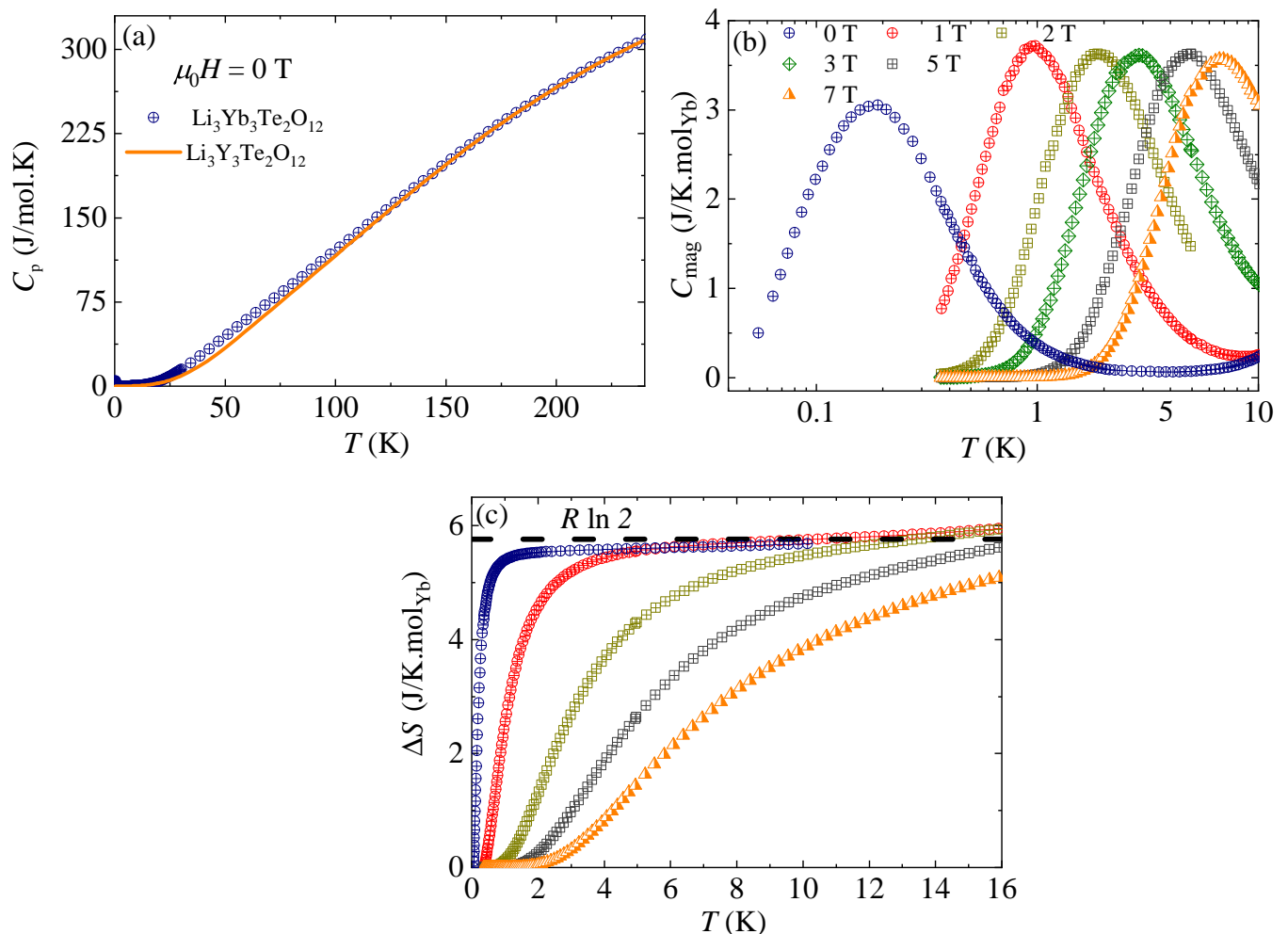


FIG. 2. Specific heat of LYTO in various magnetic fields. (a) The temperature dependence of specific heat (C_p) of LYTO and its non-magnetic analog $\text{Li}_3\text{Y}_3\text{Te}_2\text{O}_{12}$ in zero-magnetic field. (b) Low-temperature magnetic specific heat ($C_{\text{mag}}(T)$) after subtraction of lattice and nuclear contributions in zero-field as well as non-zero field. (c) The temperature dependence of entropy change ($\Delta S = \int C_{\text{mag}}(T)/T dT$, the temperatures of the color plots correspond to those in (b).) for magnetic fields up to 7 T with the expected entropy ($R \ln 2$ for spin-1/2) indicated by a black dashed line.

B. Specific heat

Fig. 2 (a) shows the total specific heat measured in zero-magnetic field. The absence of any λ -type peak suggests that there is no phase transition down to 54 mK. After subtracting the lattice contribution using the non-magnetic analog $\text{Li}_3\text{Y}_3\text{Te}_2\text{O}_{12}$ and the nuclear contribution associated with the hyperfine splitting of the Yb^{3+} nuclear spin multiplet [60], the resulting temperature dependence of magnetic specific heat, $C_{\text{mag}}(T)$ is shown in Fig. 2 (b) in the temperature range $54 \text{ mK} \leq T \leq 10 \text{ K}$. Below 2 K, the zero-field magnetic specific heat, $C_{\text{mag}}(T)$ starts increasing and shows a broad maximum around 0.18 K, which indicates the presence of short-range spin correlations between Yb^{3+} moments [28]. The presence of broad maximum around 0.18 K agrees well with the estimated CW temperature at low temperatures and it is consistent with general expectation for a quantum spin

liquid candidate [58].

In finite applied magnetic fields, it is observed that the broad maximum shifts to higher temperatures with increased field which opens gap owing to Zeeman splitting of the lowest Kramers doublet state. It is worth noting that we have not observed any suppression of $C_{\text{mag}}(T)$ in presence of magnetic field thus ruling out the presence of disorder [61]. Therefore, there is no uncertainties in Schottky contribution due to the effect of disorder in the extracted $C_{\text{mag}}(T)$ data. It is observed that the gap size increases with the increasing magnetic fields linearly (see SI Figs. 4 and 9) and the fit yields $g = 3.34 \pm 0.01$ which is consistent with that obtained Landé g -factor from bulk magnetization measurements. The magnetic field induced Zeeman gap in magnetic specific heat data is observed at very low-temperature in several rare-earth based spin-liquid candidates with relatively small exchange interactions compared to the Zeeman splitting

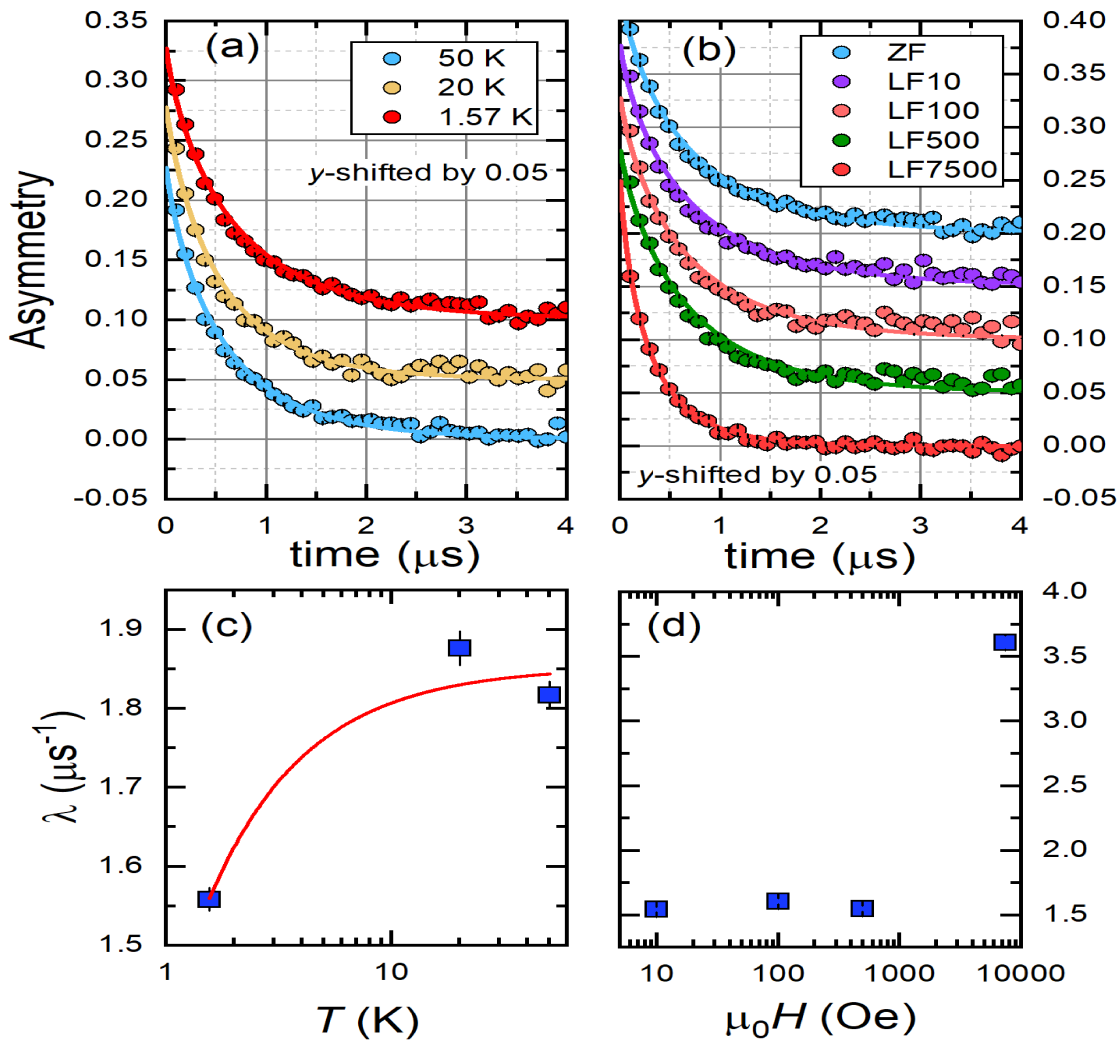


FIG. 3. μ SR data confirming a dynamic ground state in LYTO. Muon asymmetry decay obtained in ZF (a) and various LFs at 1.57 K (b) (symbols). The datasets have been shifted vertically by 0.05 for clarity. Lines are fits to a stretched exponential function (see text). The temperature (c) and longitudinal field (d) dependence of the muon spin relaxation rate λ extracted respectively from (a) and (b). The red line shows the $1/T$ -expansion of $\lambda(T)$ and indicates the presence of antiferromagnetic correlation (see text). Error bars depict an uncertainty of one standard deviation.

[37, 61].

In Fig. 2 (c), we present the estimated entropy change, ΔS , by integrating $C_{\text{mag}}(T)/T$ data in the temperature range $0.054 \text{ K} \leq T \leq 16 \text{ K}$ and $0.35 \text{ K} \leq T \leq 16 \text{ K}$ for zero-field and finite magnetic fields, respectively. The total entropy ($R \ln 2$) expected for $J_{\text{eff}} = 1/2$ state is fully recovered for zero-field as well as for non-zero magnetic fields. This provides the concrete evidence of a Kramers doublet ground state of Yb^{3+} spins in LYTO at low temperature.

C. Muon spin relaxation

We also performed muon spin relaxation (μ SR), to confirm the absence of static magnetism on a local scale.

With its spin $I = 1/2$ and gyromagnetic ratio $\gamma_{\mu}/2\pi = 135.5 \text{ MHz/T}$, an implanted muon is an unbeatably sensitive probe of magnetism. Fig. 3 shows the muon asymmetry obtained in zero (ZF) and longitudinal (LF) applied field configurations down to 1.57 K. The ZF relaxation shape is nearly exponential in the T -range 1.57-50 K. A fit of the asymmetry using a stretched exponential function $A(t) = e^{-(\lambda t)^{\beta}}$ leads to large $\beta \sim 0.8 - 1$ values. This is typical of strongly fluctuating local fields and, indeed, relaxation under LF remains almost unchanged, except for the highest field of 7500 Oe, corroborating the dynamical character of Yb^{3+} moments. We further investigated this dynamics through temperature dependence of the muon spin relaxation rate λ (Fig. 3). Above 20 K, the strong relaxation ($\sim 1.85 \mu\text{s}^{-1}$) is typical of other related $4f$ rare-earth based magnetic materials, such as

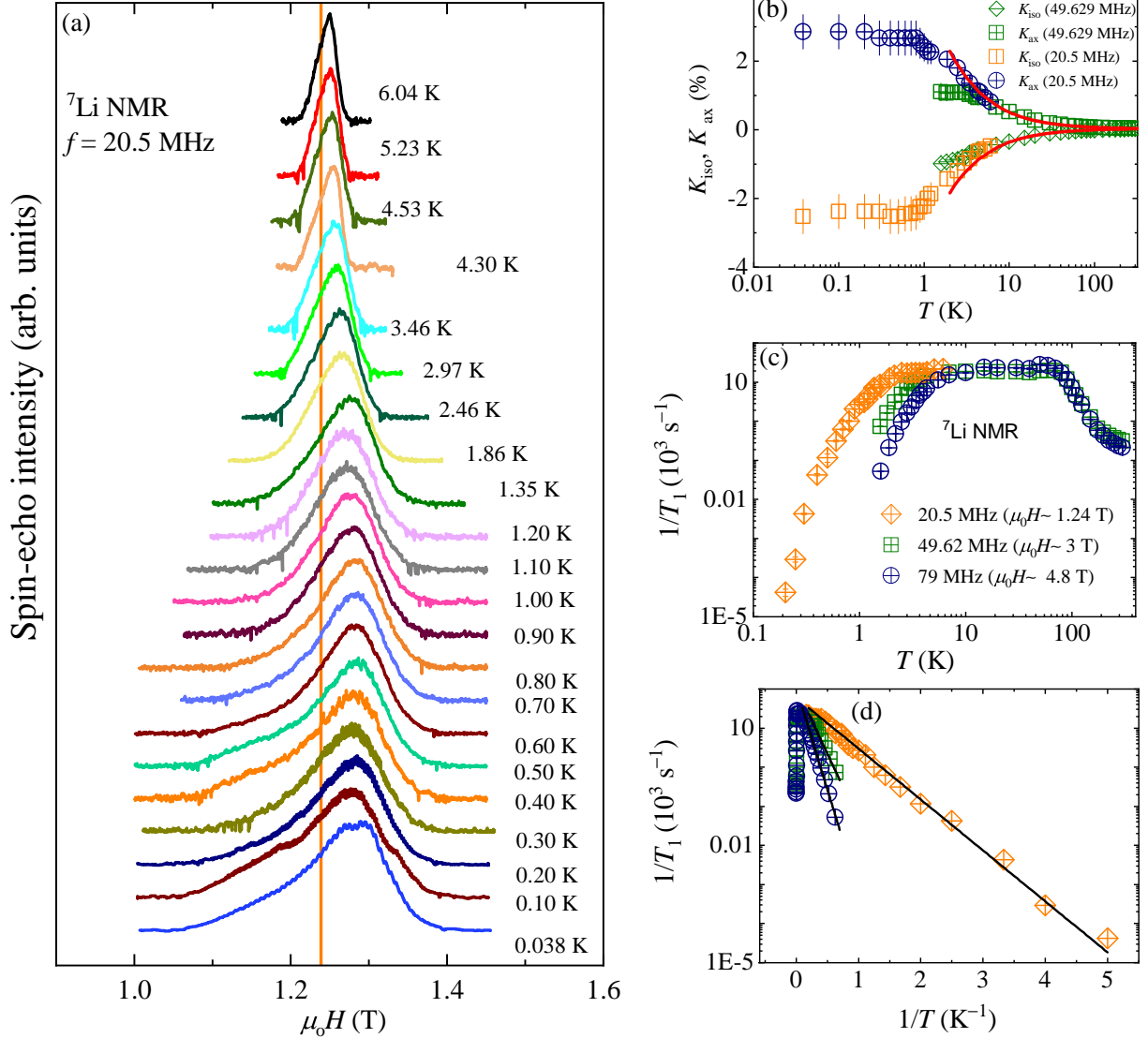


FIG. 4. ${}^7\text{Li}$ NMR spectra and spin-lattice relaxation rate in various magnetic fields reflecting the spin dynamics in the QSL state of LYTO. (a) ${}^7\text{Li}$ NMR spectra measured at constant frequency $\nu = 20.5$ MHz at a few representative temperatures. The orange vertical line corresponds to zero-shift reference line at 1.238 T. (b) The temperature dependence of isotropic (K_{iso}) and axial (K_{ax}) ${}^7\text{Li}$ NMR shifts of LYTO where the solid line is the scaled magnetic susceptibility measured in 1 T. (c) The temperature dependence of the ${}^7\text{Li}$ NMR spin-lattice relaxation rate (T_1^{-1}) for three different fields in log-log scale. (d) T_1^{-1} as a function of inverse temperature (T^{-1}) for different fields in semi-log scale. The black line represents a fit to a phenomenological model valid for thermally activated behavior of T_1^{-1} as discussed in the text. Error bars depict an uncertainty of one standard deviation.

$\text{Yb}_3\text{Ga}_5\text{O}_{12}$ or $\text{Yb}_2\text{Ti}_2\text{O}_7$, and is consistent with fast fluctuations assuming a similar local field amplitude [32]. The slight decrease of λ at low temperatures can be understood in the context of the presence of antiferromagnetic spin correlations, and the first-order $1/T$ -expansion $\lambda(T) = \lambda^{(\infty)}(1 + \theta_{\text{CW}}/T)$ [62] gives a crude estimate of $\theta_{\text{CW}} = -0.25(5)$ K (the red line in Fig. 3 (c)), in agreement with magnetization measurements.

D. Nuclear magnetic resonance

We carried out NMR experiments in LYTO in order to confirm the absence of magnetic ordering down to the lowest experimentally accessible temperatures and to track static and dynamic susceptibilities. ${}^7\text{Li}$ NMR spectra are relatively narrow at room temperature (See SI Fig. 5), however, they exhibit marked broadening below 10 K due to anisotropic interactions and the development of Yb^{3+} electron spin correlations. We observed no de-

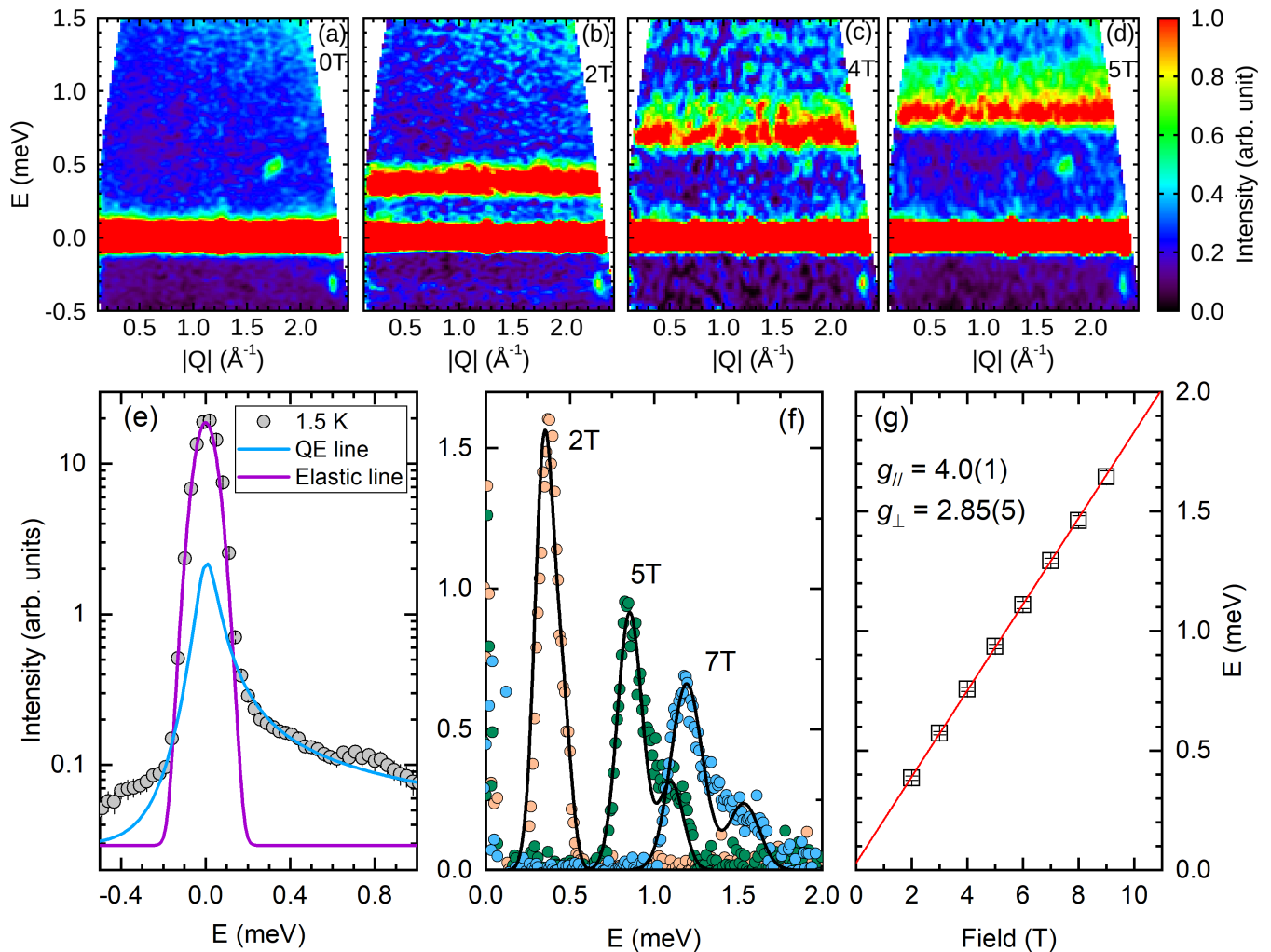


FIG. 5. Inelastic neutron scattering. (a-d) Intensity maps of the dynamical structure factor $S(Q, E)$ for polycrystalline LYTO measured at $T = 1.5$ K under zero applied field (a), $\mu_0 H = 2$ T (b), $\mu_0 H = 4$ T (c) and $\mu_0 H = 5$ T (d). (e-f) Intensity versus energy for the Q -integrated region $[0, 1.5] \text{ \AA}^{-1}$ for the zero-field dataset (e) and some selected datasets under applied fields (from which a field-independent background has been subtracted) (f). Experimental data points are symbols, purple line the estimated elastic contribution of the zero-field data and blue line is the Lorentzian quasi-elastic contribution. Solid black lines in (f) are simulations assuming an axially symmetric g -tensor (see text). (g) Median position of the spectrum as a function of the applied field (black squares). Red solid line is a linear fit.

tectable line corresponding to the satellite transitions on both sides of the central transition, which indicates the presence of a very weak quadrupole interaction. Furthermore, the line shape was found asymmetric indicating the presence of either asymmetry in the hyperfine coupling between the Li nucleus and Yb^{3+} spins or asymmetry in spin susceptibility at low-temperature, both leading to asymmetry in hyperfine fields. The smooth evolution of the NMR spectra in the entire temperature range rules out the presence of a long-range magnetic ordering at least down to 38 mK. The observation of clear shift of spectra in Fig. 4 (a) uniquely determines the intrinsic uniform static spin susceptibility on a microscopic scale. It is independent and saturates to a finite value in the low-temperature limit due to the strong polarization of

the Yb^{3+} moments under the applied magnetic field. Fig. 4 (b) presents the temperature dependence of the isotropic NMR shift, K_{iso} , and the axial shift K_{ax} , that were extracted from the fitting of NMR spectra. At high-temperatures both K_{iso} and K_{ax} scale with bulk magnetic susceptibility as expected due to significant hyperfine coupling between ${}^7\text{Li}$ nuclei and Yb atoms (see SI Fig. 7). The scaling of K with χ indicates that the macroscopic magnetization is intrinsic and originates from Yb^{3+} electronic moments while any impurity contributions are negligible. The NMR shift reveals the presence of anisotropic hyperfine field as expected for $4f$ quantum magnets possibly associated with spin-orbit interactions.

The nuclear spin-lattice relaxation rate (T_1^{-1}) probes the

wave-vector q -averaged low-energy spin excitations owing to dynamical electron spin susceptibility in the ground state of correlated quantum materials. Fig. 4 (c) shows the temperature dependence of T_1^{-1} in three different magnetic fields, which exhibits the presence of three different relaxation regimes. Upon lowering the temperature from 300 K, T_1^{-1} increases in the intermediate temperature range and exhibits a plateau around 70 K. Such increase of T_1^{-1} is not expected for paramagnetic Yb^{3+} spins but is rather due to crystal electric field effects, where spin fluctuations ν slow down with decreasing temperature and cause increased NMR relaxation in the fast fluctuation regime, where $1/T_1 \propto 1/\nu$ [63]. Below 70 K, T_1^{-1} remains constant and field-independent down to 10 K, which suggests that the relaxation is dominated by paramagnetic fluctuations of Yb^{3+} spins. At low T , i.e., below ~ 10 K depending on the field, a dramatic field dependence of T_1^{-1} develops with a decrease of the T_1^{-1} value larger than two orders of magnitude in 4.8 T compared to that in 1.24 T at 1.6 K. T_1^{-1} decreases exponentially in the temperature range $0.2 \text{ K} \leq T \leq 10 \text{ K}$, suggesting a gapped excitation spectrum. It is also observed that, T_1^{-1} drops faster in higher magnetic fields which again suggests a field-driven gap as the specific heat data does. In Fig. 4 (d), we present T_1^{-1} as a function of inverse temperature (T^{-1}) in a semi-log plot where the phenomenological model relevant for thermally activated behavior i.e., $T_1^{-1} \propto \exp(-\Delta/k_B T)$ yield a straight line with a slope proportional to the gap [63, 64]. We observe that the obtained gap indeed scales linearly with the applied magnetic field (see SI Fig. 9), which is consistent with the specific heat results. In addition, three distinct energy regimes are also observed in the spin-spin relaxation rate (T_2^{-1} ; see SI Fig. 8). The absence of any peak feature in the temperature dependence of T_1^{-1} rules out the presence of any phase transition also from the spin dynamics perspective down to 200 mK, the lowest temperature that was reached in our spin-lattice relaxation experiment. NMR results thus reveal the presence of a dynamic ground state down to 38 mK with a field-induced gap owing to Zeeman splittings of the Kramers doublet state.

E. Inelastic neutron scattering

In order to investigate in more detail the nature of excitations at low-energy, we carried out inelastic neutron scattering measurements on the cold neutron time-of-flight instrument (DCS) at the NCNR (Gaithersburg, MD). Fig. 5 shows the dynamical structure factor measured for an incident energy $E_i = 3.27 \text{ meV}$ with a resolution of 0.11 meV (FWHM). The inelastic spectrum of the zero-field dataset is essentially featureless (Fig. 5 (a)). The Q -integrated energy cut (Fig. 5 (e)) can be well fitted to an elastic Gaussian line plus a quasi-elastic Lorentzian profile, $S(Q, E) \sim (1 - e^{-E/k_B T})^{-1} E \Gamma / (E^2 + \Gamma^2)$, accounting

for the magnetic contribution. In agreement with the NMR and μSR results, the Yb^{3+} ions are found to be in a paramagnetic fluctuating regime characterized by a quasi-elastic line with the linewidth $\Gamma = 0.05(2) \text{ meV}$ setting an upper value of the energy scale of the interactions ($\sim 0.6 \text{ K}$), which is consistent with all other results. Upon increasing the field, a non-dispersive mode emerges from the elastic line (Fig. 5 b-d) whose median position depends linearly on the applied field (Fig. 5 g). It is ascribed to the Zeeman splitting of the effective spin $J_{\text{eff}} = 1/2$ of the Kramers doublet. Fig. 5 (f) shows Q -integrated energy cuts for different applied fields, which further reveal the presence of two humps whose center to center distance increases with fields. This spectrum is characteristic of an axially symmetric g -tensor [65]. To further extract the values of the g -tensor along the local anisotropy axis, $g_z = g_{\parallel}$, and in the perpendicular plane, $g_{xx} = g_{yy} = g_{\perp}$, we simulated the powder-averaged dynamical neutron structure factor (black lines in Fig. 5f) and found $g_{\parallel} = 4.0(1)$ and $g_{\perp} = 2.85(5)$, that account for all the datasets from 2 to 9 T. This leads to the powder-average value $g = \sqrt{g_{\parallel}^2/3 + 2g_{\perp}^2/3} = 3.27(7)$, which is in reasonable agreement with that obtained from other experiments.

IV. SUMMARY

In the 3D rare-earth based quantum material $\text{Li}_3\text{Yb}_3\text{Te}_2\text{O}_{12}$ featuring a perfect hyperkagome lattice constituted by Yb^{3+} ions, our results using several complementary experimental techniques reveal that Yb^{3+} realizes a Kramers doublet and hence an effective $J_{\text{eff}} = 1/2$ degrees of freedom captures the essence of the low energy physics in the ground state. The Yb^{3+} spins remain dynamic, which is characterized by quasi-elastic INS line in inelastic neutron scattering experiments and $J_{\text{eff}} = 1/2$ moments interacting with an energy of 0.6 K, which is rather low but typical for $4f$ -based quantum materials. Furthermore, ac susceptibility data show no sign of spin freezing down to 45 mK. The lack of phase transition down to 54 mK is evidenced also by the magnetic specific heat data and a broad maximum around 0.18 K in zero-field is attributed to the presence of short-range spin-correlations. The compound thus presents an interesting setting wherein geometrical frustration conspires with quantum fluctuations to evade magnetic long-range ordering as further revealed by our NMR results down to 38 mK that is consistent with ac susceptibility and specific heat results, the primary hallmark of a dynamic ground state. A field induced gap was evidenced in the specific heat, NMR relaxation rate and neutron scattering results which is reconciled with the Zeeman splitting of the effective spin $J_{\text{eff}} = 1/2$ of the Kramers doublet. The $4f$ moments on a hyperkagome lattice- an emblematic frustrated three dimensional model offer a rare

realization of a spin liquid. Our comprehensive results demonstrate a liquid-like dynamic state in a rare-earth hyperkagome, which might open the possibility of stabilizing spin-orbit driven quantum disordered state in $4f$ magnets. This new family of rare-earth hyperkagome quantum material $\text{Li}_3\text{RE}_3\text{Te}_2\text{O}_{12}$ holds great potential to realize spin-orbit driven quantum phenomena and opens new avenues for modern theoretical approaches in establishing generic frameworks in the context of spin liquids.

V. ACKNOWLEDGMENTS

We acknowledge stimulating discussions with P. Mendels. PK acknowledges the funding by the Science

and Engineering Research Board, and Department of Science and Technology, India through Research Grants. This research was supported by the U.S. Department of Energy, Office of Basic Energy Sciences, Division of Materials Sciences and Engineering. Ames Laboratory is operated for the U.S. Department of Energy by Iowa State University under Contract No. DE-AC02-07CH11358. EK and SB acknowledges the France Canada Research Fund for financial support. AZ acknowledges the financial support of the Slovenian Research agency under program No. P1-0125 and projects No. J1-2461 and No. N1-0148. AMS thanks the URC/FRC of UJ and the SA-NRF for financial support.

-
- [1] *Editorial.*, *Nat. Phys.* **12**, 105 (2016).
- [2] Y. Tokura, M. Kawasaki, and N. Nagaosa, *Nat. Phys.* **13**, 1056 (2017).
- [3] D. N. Basov, R. D. Averitt, and D. Hsieh, *Nat. Mater.* **16**, 1077 (2017).
- [4] B. Keimer and J. E. Moore, *Nat. Phys.* **13**, 1045 (2017).
- [5] P. Anderson, *Mater. Res. Bull.* **8**, 153 (1973).
- [6] L. Balents, *Nature (London)* **464**, 199 (2010).
- [7] M. J. P. Gingras and P. A. McClarty, *Rep. Prog. Phys.* **77**, 056501 (2014).
- [8] H. Takagi, T. Takayama, G. Jackeli, G. Khaliullin, and S. E. Nagler, *Nat. Rev. Phys.* **1**, 264 (2019).
- [9] M. R. Norman, *Rev. Mod. Phys.* **88**, 041002 (2016).
- [10] C. Nayak, S. H. Simon, A. Stern, M. Freedman, and S. Das Sarma, *Rev. Mod. Phys.* **80**, 1083–1159 (2008).
- [11] L. Savary and L. Balents, *Rep. Prog. Phys.* **80**, 016502 (2016).
- [12] C. Broholm, R. J. Cava, S. A. Kivelson, D. G. Nocera, M. R. Norman, and T. Senthil, *Science* **367** (2020), 10.1126/science.aay0668.
- [13] Y. Zhou, K. Kanoda, and T.-K. Ng, *Rev. Mod. Phys.* **89**, 025003 (2017).
- [14] M. Klanjšek, A. Zorko, R. Žitko, J. Mravlje, Z. Jagličić, P. K. Biswas, P. Prelovšek, D. Mihailovic, and D. Arčon, *Nat. Phys.* **13**, 1130 (2017).
- [15] Y. Li, D. Adroja, P. K. Biswas, P. J. Baker, Q. Zhang, J. Liu, A. A. Tsirlin, P. Gegenwart, and Q. Zhang, *Phys. Rev. Lett.* **117**, 097201 (2016).
- [16] P. Khuntia, M. Velazquez, Q. Barthélemy, F. Bert, E. Kermarrec, A. Legros, B. Bernu, L. Messio, A. Zorko, and P. Mendels, *Nat. Phys.* **16**, 469 (2020).
- [17] T.-H. Han, J. S. Helton, S. Chu, D. G. Nocera, J. A. Rodriguez-Rivera, C. Broholm, and Y. S. Lee, *Nature* **492**, 406 (2012).
- [18] B. Bernu, C. Lhuillier, and L. Pierre, *Phys. Rev. Lett.* **69**, 2590 (1992).
- [19] Z. Zhu, P. A. Maksimov, S. R. White, and A. L. Chernyshev, *Phys. Rev. Lett.* **119**, 157201 (2017).
- [20] P. Khuntia, R. Kumar, A. V. Mahajan, M. Baenitz, and Y. Furukawa, *Phys. Rev. B* **93**, 140408 (2016).
- [21] J. Knolle and R. Moessner, *Annu. Rev. Condens. Matter Phys.* **10**, 451 (2019).
- [22] P. Khuntia, F. Bert, P. Mendels, B. Koteswararao, A. V. Mahajan, M. Baenitz, F. C. Chou, C. Baines, A. Amato, and Y. Furukawa, *Phys. Rev. Lett.* **116**, 107203 (2016).
- [23] S. Chillal, Y. Iqbal, H. O. Jeschke, J. A. Rodriguez-Rivera, R. Bewley, P. Manuel, D. Khalyavin, P. Steffens, R. Thomale, A. T. M. N. Islam, J. Reuther, and B. Lake, *Nat. Commun* **11**, 2348 (2020).
- [24] T. Arh, B. Sana, M. Pregelj, P. Khuntia, Z. Jagličić, M. D. Le, P. K. Biswas, P. Manuel, L. Mangin-Thro, A. Ozarowski, and A. Zorko, *Nat. Mater.* **21**, 416 (2022).
- [25] W. Witczak-Krempa, G. Chen, Y. B. Kim, and L. Balents, *Annu. Rev. Condens. Matter Phys.* **5**, 57 (2014).
- [26] P. A. Maksimov, Z. Zhu, S. R. White, and A. L. Chernyshev, *Phys. Rev. X* **9**, 021017 (2019).
- [27] A. P. Ramirez, A. Hayashi, R. J. Cava, R. Siddharthan, and B. S. Shastry, *Nature* **399**, 333 (1999).
- [28] M. B. Bordelon, E. Kenney, C. Liu, T. Hogan, L. Posthuma, M. Kavand, Y. Lyu, M. Sherwin, N. P. Butch, C. Brown, M. J. Graf, L. Balents, and S. D. Wilson, *Nat. Phys.* **15**, 1058 (2019).
- [29] Y. Taguchi, Y. Oohara, H. Yoshizawa, N. Nagaosa, and Y. Tokura, *Science* **291**, 2573 (2001).
- [30] Y. Machida, S. Nakatsuji, S. Onoda, T. Tayama, and T. Sakakibara, *Nature* **463**, 210 (2010).
- [31] G. Hester, H. S. Nair, T. Reeder, D. R. Yahne, T. N. DeLazzer, L. Berges, D. Ziat, J. R. Neilson, A. A. Aczel, G. Sala, J. A. Quilliam, and K. A. Ross, *Phys. Rev. Lett.* **123**, 027201 (2019).
- [32] P. Dalmas de Réotier, A. Yaouanc, P. C. M. Gubbens, C. T. Kaiser, C. Baines, and P. J. C. King, *Phys. Rev. Lett.* **91**, 167201 (2003).
- [33] H. J. Silverstein, K. Fritsch, F. Flicker, A. M. Hallas, J. S. Gardner, Y. Qiu, G. Ehlers, A. T. Savici, Z. Yamani, K. A. Ross, B. D. Gaulin, M. J. P. Gingras, J. A. M. Paddison, K. Foyevtsova, R. Valenti, F. Hawthorne, C. R. Wiebe, and H. D. Zhou, *Phys. Rev. B* **89**, 054433 (2014).
- [34] T. Fennell, P. P. Deen, A. R. Wildes, K. Schmalzl, D. Prabhakaran, A. T. Boothroyd, R. J. Aldus, D. F. McMorrow, and S. T. Bramwell, *Science* **326**, 415 (2009).
- [35] S. Petit, E. Lhotel, B. Canals, M. Ciomaga Hatnean, J. Ollivier, H. Mutka, E. Ressouche, A. R. Wildes, M. R. Lees, and G. Balakrishnan, *Nat. Phys.* **12**, 746 (2016).

- [36] S. T. Bramwell and M. J. P. Gingras, *Science* **294**, 1495 (2001).
- [37] B. Gao, T. Chen, D. W. Tam, C.-L. Huang, K. Sasmal, D. T. Adroja, F. Ye, H. Cao, G. Sala, M. B. Stone, C. Baines, J. A. T. Verezhak, H. Hu, J.-H. Chung, X. Xu, S.-W. Cheong, M. Nallaiyan, S. Spagna, M. B. Maple, A. H. Nevidomskyy, E. Morosan, G. Chen, and P. Dai, *Nat. Phys.* **15**, 1052 (2019).
- [38] R. Sibille, N. Gauthier, E. Lhotel, V. Porée, V. Pomjakushin, R. A. Ewings, T. G. Perring, J. Ollivier, A. Wildes, C. Ritter, T. C. Hansen, D. A. Keen, G. J. Nilsen, L. Keller, S. Petit, and T. Fennell, *Nat. Phys.* **16**, 546 (2020).
- [39] J. A. M. Paddison, H. Jacobsen, O. A. Petrenko, M. T. Fernández-Díaz, P. P. Deen, and A. L. Goodwin, *Science* **350**, 179 (2015).
- [40] L. O. Sandberg, R. Eddberg, I.-M. B. Bakke, K. S. Pedersen, M. C. Hatnean, G. Balakrishnan, L. Mangin-Thro, A. Wildes, B. Fåk, G. Ehlers, G. Sala, P. Henelius, K. Lefmann, and P. P. Deen, *Phys. Rev. B* **104**, 064425 (2021).
- [41] Y. Cai, M. N. Wilson, J. Beare, C. Lygouras, G. Thomas, D. R. Yahne, K. Ross, K. M. Taddei, G. Sala, H. A. Dabkowska, A. A. Aczel, and G. M. Luke, *Phys. Rev. B* **100**, 184415 (2019).
- [42] N. Zhao, H. Ge, L. Zhou, Z. M. Song, J. Yang, T. T. Li, L. Wang, Y. Fu, Y. F. Zhang, J. B. Xu, S. M. Wang, J. W. Mei, X. Tong, L. S. Wu, and J. M. Sheng, *Phys. Rev. B* **105**, 014441 (2022).
- [43] D. G. Onn, H. Meyer, and J. P. Remeika, *Phys. Rev.* **156**, 663 (1967).
- [44] P. P. Deen, O. Florea, E. Lhotel, and H. Jacobsen, *Phys. Rev. B* **91**, 014419 (2015).
- [45] R. Wawrzyńczak, B. Tomasello, P. Manuel, D. Khalyavin, M. D. Le, T. Guidi, A. Cervellino, T. Ziman, M. Boehm, G. J. Nilsen, and T. Fennell, *Phys. Rev. B* **100**, 094442 (2019).
- [46] X. G. Wen, F. Wilczek, and A. Zee, *Phys. Rev. B* **39**, 11413 (1989).
- [47] R. Shindou, *Phys. Rev. B* **93**, 094419 (2016).
- [48] M. Hermele, M. P. A. Fisher, and L. Balents, *Phys. Rev. B* **69**, 064404 (2004).
- [49] S.-S. Gong, W. Zheng, M. Lee, Y.-M. Lu, and D. N. Sheng, *Phys. Rev. B* **100**, 241111 (2019).
- [50] F. A. Cevallos, S. Guo, and R. J. Cava, *Mater. Res. Express* **5**, 126106 (2018).
- [51] B. H. Toby, *J. Appl. Cryst.* **34**, 210 (2001).
- [52] Y. Shimizu, H. Takeda, M. Tanaka, M. Itoh, S. Niitaka, and H. Takagi, *Nat. Commun.* **3**, 981 (2012).
- [53] A. P. Dioguardi, S. Selter, U. Peeck, S. Aswartham, M.-I. Sturza, R. Murugesan, M. S. Eldeeb, L. Hozoi, B. Büchner, and H.-J. Grafe, *Phys. Rev. B* **102**, 064429 (2020).
- [54] S. Toth and B. Lake, *J. Phys. Condens. Matter* **27**, 166002 (2015).
- [55] R. Sibille, E. Lhotel, V. Pomjakushin, C. Baines, T. Fennell, and M. Kenzelmann, *Phys. Rev. Lett.* **115**, 097202 (2015).
- [56] K. A. Ross, L. Savary, B. D. Gaulin, and L. Balents, *Phys. Rev. X* **1**, 021002 (2011).
- [57] J. Xing, L. D. Sanjeewa, J. Kim, G. R. Stewart, M.-H. Du, F. A. Reboredo, R. Custelcean, and A. S. Sefat, *ACS Mater. Lett.* **2**, 71 (2020).
- [58] P. M. Sarte, K. Cruz-Kan, B. R. Ortiz, K. H. Hong, M. M. Bordelon, D. Reig-i Plessis, M. Lee, E. S. Choi, M. B. Stone, S. Calder, D. M. Pajerowski, L. Mangin-Thro, Y. Qiu, J. P. Attfield, S. D. Wilson, C. Stock, H. D. Zhou, A. M. Hallas, J. A. M. Paddison, A. A. Aczel, and C. R. Wiebe, *npj Quantum Materials* **6**, 42 (2021).
- [59] R. Zhong, S. Guo, G. Xu, Z. Xu, and R. J. Cava, *Proc. Natl. Acad. Sci.* **116**, 14505 (2019).
- [60] A. Steppke, M. Brando, N. Oeschler, C. Krellner, C. Geibel, and F. Steglich, *Phys. Status Solidi B (b)* **247**, 737 (2010).
- [61] Z.-F. Ding, Y.-X. Yang, J. Zhang, C. Tan, Z.-H. Zhu, G. Chen, and L. Shu, *Phys. Rev. B* **98**, 174404 (2018).
- [62] P. D. de Réotier and A. Yaouanc, *J. Phys. Condens. Matter* **9**, 9113 (1997).
- [63] K. Y. Zeng, L. Ma, Y. X. Gao, Z. M. Tian, L. S. Ling, and L. Pi, *Phys. Rev. B* **102**, 045149 (2020).
- [64] J. A. Quilliam, F. Bert, E. Kermarrec, C. Payen, C. Guillot-Deudon, P. Bonville, C. Baines, H. Luetkens, and P. Mendels, *Phys. Rev. Lett.* **109**, 117203 (2012).
- [65] A. Abragam and B. Bleaney, *Electron paramagnetic resonance of transition ions* (Oxford University Press, 2012).